1   **Winter 2018 major sudden stratospheric warming impact on midlatitude mesosphere**

2   **from microwave radiometer measurements**

4   Yuke Wang[1], Valerii Shulga[1,2], Gennadi Milinevsky[1,3], Aleksey Patoka[2], Oleksandr

5   Evtushevsky[3], Andrew Klekociuk[4,5], Wei Han[1], Asen Grytsai[3], Dmitry Shulga[2], Valery

6   Myshenko[2], Oleksandr Antyufeyev[2]

8   [1]College of Physics, International Center of Future Science, Jilin University, Changchun,

9   130012, China

10   [2]Institute of Radio Astronomy, NAS of Ukraine, Kharkiv, 61002, Ukraine

11   [3]Taras Shevchenko National University of Kyiv, Kyiv, 01601, Ukraine

12   [4]Antarctica and the Global System, Australian Antarctic Division, Kingston, 7050, Australia

13   [5]Department of Physics, University of Adelaide, Adelaide, 5005, Australia

15   *Correspondence to*:

16   Gennadi Milinevsky (genmilinevsky@gmail.com) and Valerii Shulga

17   (shulga@rian.kharkov.ua)

19   **Abstract.** The impact of a major sudden stratospheric warming (SSW) in the Arctic in

20   February 2018 on the mid-latitude mesosphere is investigated by performing the microwave

21   radiometer measurements of carbon monoxide (CO) and zonal wind above Kharkiv, Ukraine

22   (50.0°N, 36.3°E). The mesospheric peculiarities of this SSW event were observed using a

23   recently designed and installed microwave radiometer in East Europe for the first time. Data

24   from the ERA-Interim and MERRA-2 reanalyses, as well as the Aura Microwave Limb

25   Sounder measurements, are also used. Microwave observations of the daily CO profiles in

26   January–March 2018 allowed the retrieval of mesospheric zonal wind at 70–85 km (below the

27   winter mesopause) over the Kharkiv site. Reversal of the mesospheric westerly from about 10

28   m s^{-1} to an easterly wind of about –10 m s^{-1} around 10 February was observed. The local

29   microwave observations at our NH midlatitude site combined with reanalysis data show wide

30   ranging daily variability in CO, zonal wind and temperature in the mesosphere and stratosphere

31   during the SSW of 2018. The observed local CO variability can be explained mainly by

32   horizontal air mass redistribution due to planetary wave activity. Replacement of the CO-rich

33   polar vortex air by CO-poor air of the surrounding area led to a significant mesospheric CO

34   decrease over the station during the SSW and fragmentation of the vortex over the station at the

35   SSW start caused enhanced stratospheric CO at about 30 km. The results of microwave

measurements of CO and zonal wind in the midlatitude mesosphere at 70–85 km altitudes, which still is not adequately covered by ground-based observations, are useful for improving our understanding of the SSW impacts in this region.

1 Introduction

Major sudden stratospheric warming (SSW) events which happen roughly every other year in the North Polar region are produced by strong planetary wave activity according to the model developed by Matsuno (1971) which is supported by numerous observations (Alexander and Shepherd, 2010; Kuttippurath and Nikulin, 2012; Tao et al., 2015). A major SSW event is accompanied by a sharp increase of the stratosphere temperature up to 50 K and the reversal of the zonal wind from climatological westerlies to easterlies over a period of several days (Charlton and Polvani, 2007; Chandran and Collins, 2014; Hu et al., 2014; Tripathi et al., 2016; Butler et al., 2017; Karpechko et al., 2018; Taguchi, 2018; Rao et al., 2018). The primary definition of a SSW event provided by the World Meteorological Organization requires a stratosphere temperature increase and an accompanying zonal wind reversal to easterlies at the 10-hPa pressure level (approximately 30 km altitude) and 60° latitude (WMO, 1978). This definition was broadened and detailed in recent papers (Butler et al., 2015; Butler and Gerber, 2018; Rao et al., 2019). The summarizing paper, where a SSW database is described, was published in Butler et al. (2017). This useful tool (https://www.esrl.noaa.gov/csd/groups/csd8/sswcompendium/) allows analysis of the conditions in the stratosphere, troposphere, and at the surface before, during and after each SSW event representing its evolution, structure, and impact on winter surface climate. The compendium is based on data from six different reanalysis products, covers the 1958–2014 period and includes global daily anomaly fields, full fields, and derived products for each SSW event (Butler et al., 2017).

The source of the SSW is planetary wave activity born in the troposphere that propagates upward through the tropopause to the stratosphere (Matsuno, 1971; Alexander and Shepherd, 2010, Butler et al., 2015). The enhanced wave activity results in the rapid warming of the polar stratosphere and the breakdown of the stratospheric polar vortex (Matsuno, 1971; de la Torre et al., 2012; Chandran and Collins, 2014; Pedatella et al., 2018). The important feature of a SSW event is its impact on lower altitudes, when temperature and wind anomalies descend downward into the high- and mid-latitude troposphere during the following weeks to month and influence the surface weather (Baldwin and Dunkerton, 2001; Zhou et al., 2002; Butler et

al., 2015; Yu et al., 2018). The major SSW events may also impact the atmospheric composition of the whole Northern Hemisphere (NH) stratosphere including mid-latitudes (Solomon et al., 1985; Allen et al., 1999; Tao et al., 2015).

During the SSW, vertical coupling covers not only the troposphere but extends upward to the mesosphere. Mesospheric responses to the SSW are observed as enhancement in planetary wave amplitude, zonal wind reversal and significant air cooling (Shepherd et al., 2014; Zülicke and Becker, 2013; Stray et al., 2015; Zülicke et al., 2018), substantial depletion of the metal layers (Feng et al., 2017; Gardner, 2018), mesosphere-to-stratosphere descent of trace species (Manney et al., 2009; Salmi et al., 2011). The SSW events are also accompanied by the rapid descent of the stratopause into the stratosphere at the SSW onset, followed by formation of the elevated stratopause in the lower mesosphere and gradual stratopause lowering toward its typical position in the SSW recovery phase (Manney et al., 2009; Chandran et al., 2011; Salmi et al., 2011; Tomikawa et al., 2012; Limpasuvan et al., 2016; Orsolini et al., 2010, 2017). The elevated stratopause events provide an evidence of the coupling between the stratosphere and the mesosphere.

Among the trace gases, the CO molecule is a good tracer of winter polar vortex dynamics in the upper stratosphere and mesosphere due to its long photochemical lifetime (Solomon et al., 1985; Allen et al., 1999; Rinsland et al., 1999, Shepherd et al. 2014). The CO mixing ratio generally increases with height in the upper stratosphere and mesosphere and increases with latitude toward the winter pole. This is due to the mean meridional circulation which transports CO from the source region in the summer hemisphere and tropics to the extratropical winter mesosphere and stratosphere (Shepherd et al., 2014). Therefore, large abundances of CO appear in the winter polar regions under conditions of large-scale planetary wave activity. Downward meridional transport causes descent of CO between the mesosphere and stratosphere and this process is sensitive to planetary wave amplitudes, and particularly the wave amplitude changes that occur during SSWs (Rinsland et al., 1999; Manney et al., 2009; Kvissel et al., 2012). Due to the large scale descent, high CO values of mesospheric origin are observed at stratospheric altitudes down to 25–30 km (Engel et al., 2006; Huret et al., 2006; Funke et al., 2009). At NH mid-latitudes, CO also exhibits significant variability during periods of planetary wave activity associated with SSWs, when the polar vortex splits and displaces off the pole (Solomon et al., 1985; Allen et al., 1999; Funke et al., 2009).

Recent atmospheric models are being extended up to 80–150 km and are used for the study of SSWs (de la Torre et al., 2012; Chandran and Collins, 2014; Shepherd at al., 2014; Limpasuvan et al., 2016; Newnham et al., 2016). For example, de la Torre et al. (2012) applied the Whole Atmosphere Community Climate Model (WACCM) and Shepherd at al. (2014) used

106 the Canadian Middle Atmosphere Model (CMAM) for SSW modeling. The reference wind

107 profiles for the models are mainly retrieved from observations of the radiation of the

108 mesospheric ozone molecules, which allow robust measurements at altitudes up to of

109 approximately 65 km (e.g., Hagen et al., 2018). These data are generally consistent with the

110 most commonly used reanalysis products. However, there are still insufficient observations of

111 middle atmospheric winds at altitudes between 60 and 85 km made with a high vertical

112 resolution to verify atmospheric models and possible long-term trends (Keuer et al., 2007;

113 Hagen et al., 2018; Rüfenacht et al., 2018). This altitude range, where temperature generally

114 decreases with height, which causes inherent vertical instability, is situated below the winter

115 mesopause region at 95–100 km (e.g. Xu et al., 2009) and plays a significant role in the mass

116 and energy exchange between the stratosphere and the mesosphere (Shepherd et al., 2014;

117 Limpasuvan et al., 2016; Gardner, 2018).

118   Microwave radiometry is a ground-based technique that can provide vertical profiles of CO,

119 H_2O and O_3 atmospheric gases and wind data in the upper stratosphere and mesosphere

120 (Rüfenacht et al., 2012; Scheiben et al., 2012; Forkman et al., 2016). The upper stratosphere–

121 mesosphere zonal winds at the 30–85 km altitude region can be measured using the Doppler

122 shift between different observation directions in simultaneously measured spectra of transitions

123 lines of carbon monoxide at 115.3 GHz and ozone O_3 at 110.8 GHz (Rüfenacht et al., 2012;

124 Forkman et al., 2016). Due to high altitude CO residence region, the simultaneous zonal wind

125 measurements using both O_3 and CO provide independent data that extend the wind

126 measurement from the stratospheric to mesospheric altitudes, respectively (Forkman et al.,

127 2016; Piddyachiy et al., 2017).

128   The first ground-based microwave measurements of CO were made in the 1970s and they

129 confirmed theoretical estimations of the vertical CO profile (Waters et al., 1976; Goldsmith et

130 al., 1979). Since the 1990s, the ground-based microwave radiometers measuring CO have been

131 installed in the Northern Hemisphere at high and middle latitudes to provide measurements on

132 a regular basis. Microwave radiometers are operating in Onsala and Kiruna, Sweden, since

133 2008. The results are described in Hoffmann et al. (2011) and in Forkman et al. (2012). The

134 microwave radiometer operated in Bern, Switzerland since 2010 aims to contribute to the

135 significant gap that exists in the middle atmosphere between 40 and 70 km altitude for wind

136 data (Rüfenacht et al., 2012). In the Arctic, the O_3, N_2O, HNO_3, and CO spectra were recorded

137 using the Ground-Based Millimetre-wave Spectrometer GBMS (Muscari et al., 2007; Di Biagio

138 et al., 2010).

139   Since 2014, the microwave measuring system for CO observations has been operated in

140 Kharkiv, Ukraine (Piddyachiy et al., 2010; Piddyachiy et al., 2017). Microwave radiometer

measurements of CO are used to retrieve mesospheric winds nearby the mesopause region (70–85 km). Methods deriving the wind speed from mesospheric CO measurements are based on the determination of the CO and O_3 lines emission Doppler shift (Eriksson et al., 2011; Hagen et al., 2018).

Our observations in February 2018 using the new microwave radiometer at the mid-latitude Kharkiv station have recorded the mesospheric effects of a major SSW. In mid-February 2018, the stratospheric polar vortex in the Arctic splitted into two sister vortices (Fig. 1), the zonal wind reversed in the stratosphere–mesosphere from westerly to easterly and warm air penetrated into the polar cap regions (Rao et al., 2018; Karpechko et al., 2018; Vargin and Kiryushov, 2019). This caused large-scale disturbances in the middle atmosphere of the polar and middle latitudes. The major SSW in 2018 is not yet widely discussed in publications (Rao et al., 2018; Karpechko et al., 2018; Vargin and Kiryushov, 2019) and in this paper, we give a detailed description of the observed mesospheric CO and zonal wind variations.

In Sect. 2, the microwave radiometer and data processing software are briefly described. The SSW event in February 2018 is considered in Sect. 3. The effects of the SSW on mid-latitude mesosphere–stratosphere conditions in the Ukraine longitudinal sector are presented in Sect. 4. Discussion is given in Sect. 5 followed by conclusions in Sect. 6.

2 Data and methods

The microwave radiometer data set registered during the 2017/2018 winter campaign in Kharkiv (50.0°N, 36.3°E) is used in this study to investigate local effects of the winter 2018 sudden stratospheric warming on the mesosphere and stratosphere. Since the ground-based microwave measurements are spatially limited by instrument coverage, data on air temperature, zonal wind and geopotential height were used from reanalyses and satellite databases to interpret the CO profile and the zonal wind microwave observations and to describe the SSW effects in the atmosphere of the surrounding mid-latitude region (30–40°E, 48–52°N).

2.1 Microwave radiometer, method, and midlatitude data description

The microwave radiometer (MWR) with high sensitivity, installed at Kharkiv, Ukraine, is designed for continuous observations of the atmospheric CO profiles and zonal wind speed in the mesosphere using emission lines at 115.3 GHz. The radiometer can continuously provide

176   vertical profiles up to the mesopause region during day and night, even in cloudy conditions

177   (Hagen et al., 2018). However, precipitation, such as strong rain or snow, can prevent the

178   measurements.

179   The receiver of the radiometer has the double-sideband noise temperature of 250 K at an

180   ambient temperature of 10°C (Piddyachiy et al., 2010; 2017). The radiometer was tested during

181   the 2014–2015 period for observation of the CO emission lines in the mesosphere over Kharkiv.

182   These tests proved the reliability of the receiver system, on which further details are provided

183   in Piddyachiy et al. (2017). Since 2015, the radiometer has been used for continuous

184   microwave measurements of CO profiles and mesosphere wind investigations. The first

185   observations of the atmospheric CO spectral lines over Kharkiv have confirmed seasonal

186   variations in the CO abundance (Piddyachiy et al., 2017). Operation of the MWR in a double-

187   sideband mode allows retrieval of wind speed from the Doppler shift of the CO line emission at

188   the 115.3 GHz. Two methods are used to determine wind speed. Firstly the observed line shape

189   is fitted by a Voigt profile and the center frequency is determined (Piddyachiy et al., 2017).

190   Secondly radiative transfer calculations for a horizontally layered atmosphere are used to

191   determine the wind profiles with the Qpack package, version 1.0.93 (Eriksson et al., 2005;

192   Eriksson et. al., 2011), which is specifically designed to work with the forward model of the

193   Atmospheric Radiative Transfer Simulator ARTS (Buehler et al., 2018;

194   http://www.radiativetransfer.org/). The results obtained by both methods were almost the same

195   within the error limits. In this paper, both methods were used and provided average values of

196   the zonal wind speed for altitudes of 70–85 km. The time interval of the data used here was

197   January 1 – March 31, 2018, which covers the main phases of the SSW 2018 event.

198

199

200   **2.2 Data from other sources**

201

202   In this study, daily datasets from ERA-Interim global atmospheric reanalysis of European

203   Centre for Medium-Range Weather Forecast (ECMWF; Dee et al., 2011) were downloaded

204   from (https://www.ecmwf.int/en/forecasts/datasets/archive-datasets/reanalysis-datasets/era-

205   interim) and have been used for comparison with MWR observations. The ERA-Interim data

206   were used to create temperature and zonal wind velocity profiles and to calculate geopotential

207   height at the stratospheric pressure levels, in order to compare with the data measured over the

208   Kharkiv site. Aura Microwave Limb Sounder (MLS) measurements of the air temperature were

209   analyzed as well (Xu et al., 2009; https://mls.jpl.nasa.gov/data/readers.php; see details in the

210   Supplement).

211   Zonal wave amplitudes in geopotential height were analyzed using the National Oceanic and
212   Atmospheric Administration National Centers for Environmental Prediction, Global Data
213   Assimilation System–Climate Prediction Center (NOAA NCEP GDAS–CPC) data at
214   https://www.cpc.ncep.noaa.gov/products/stratosphere/strat-trop/ and the MERRA-2 data from
215   the National Aeronautics and Space Administration Goddard Space Flight Center, Atmospheric
216   Chemistry and Dynamics Laboratory (NASA GFC ACDL) site at https://acd-
217   ext.gsfc.nasa.gov/Data_services/met/ann_data.html. The detailed description of the data used
218   for analysis is given in the Supplement.

219

220

221   **3 Northern Hemisphere SSW effects**

222

223   Descending air masses are observed throughout the mesosphere and stratosphere of the winter
224   polar region (Orsolini et al., 2010; Chandran and Collins, 2014; Limpasuvan et al., 2016;
225   Zülicke et al., 2018). From Aura MLS vertical profiles, a layered descending sequence of
226   alternating cool and warm anomalies over the polar cap was observed in the 2017/2018 winter
227   (Fig. 2a). The SSW event in Fig. 2a is identified by the rapid warming in the stratosphere and
228   cooling in the mesosphere (upward arrow) starting from 10 February 2018 (left vertical line).
229   This event was preceded by progressively descending warm and cold anomalies that formed
230   in January (black and white dashed arrows, respectively). Oscillations in the intensity of the
231   anomalies indicate that they were formed under the influence of large amplitude planetary
232   waves of zonal wave numbers 1 and 2 (Fig. 2c–2e). From 1 January to 10 February (during 41
233   days), descending warm anomalies with a velocity -850 m·day^{-1} were apparent in the
234   mesosphere and the upper stratosphere (75 to 40 km; black dashed arrow in Fig. 2a). Below the
235   warm anomaly, a cold anomaly descended between the upper and lower stratosphere (45 to 20
236   km) with velocity -600 m·day^{-1} (white dashed arrow in Fig. 2a), while a cold mesospheric
237   anomaly in February–March descended with average velocity -750 m·day^{-1} (white dotted
238   arrow in Fig. 2a). Our velocity estimates are similar to those of Salmi et al. (2011) who found
239   that mesospheric NO_x anomalies during the major SSW 2009 were transported from 80 to 55
240   km in about 40 days, i.e. with velocity -600 m·day^{-1}.
241   The splitting of the polar vortex (Fig. 1) and the zonal wind reversal (Fig. 2b) started at the
242   time of the wave 2 pulse on 10 February (Fig. 2d and dashed curve in Fig. 2e). Note that this is
243   close to the SSW timing in Rao et al. (2018) and Vargin and Kiryushov (2019), where the SSW
244   onset date was 11 February. As seen from Fig. 2c and solid curve in Fig. 2e, increasing wave 1
245   amplitude contributed to the destabilization of the polar vortex during January–early February

246   and to temperature and zonal wind oscillations in the mesosphere and stratosphere (Fig. 2a and
247   2b). These oscillations are usually associated with the propagation of planetary waves in the
248   stratosphere and mesosphere (Limpasuvan et al., 2016; Rüfenacht et al., 2016). As noted in an
249   earlier study (Manney et al., 2009; Rao et al., 2018), wave 1 amplitudes were also larger prior
250   to the SSW in 2009, suggesting a role of preconditioning. During 10–15 February, the easterly
251   zonal wind anomaly at the stratopause (about 1 hPa, ~50 km) increased to –60 m s^{-1} (Fig. 2b).
252   At the same time, warming in the polar stratosphere with the largest temperature anomaly of
253   about 20 K was observed between 25 and 45 km in the same time interval (upward arrow in
254   Fig. 2a). Both anomaly peaks are close in time to the wave 1 pulse after the SSW start (Fig. 2c
255   and 2e). The descending negative temperature anomaly in the mesosphere between 50 and 90
256   km persisted during and after the SSW and reached –15 K (dotted arrow in Fig. 2a).
257
258
259   **4 The local SSW effects over the midlatitude station**
260
261   **4.1 CO variability**
262
263   Local variability in the conditions of the atmosphere during the microwave measurements in
264   January–March 2018 at Kharkiv (50.0°N, 36.3°E) is shown in Figs. 3–6. The sharp changes
265   occurred in the 20-day interval from 10 February to 1 March coinciding with the SSW event
266   2018, as indicated by red vertical lines in Figs. 3, 5 and 6. At this time the polar vortex divided
267   into two parts producing two smaller vortices over the longitudinal sectors of North America
268   and Eurasia (Fig. 1). Due to the planetary wave influence (Fig. 2c–2e), the two sub-vortices
269   shifted zonally and meridionally, so that the SSW effects were observed not only in the polar
270   region but also in the middle latitudes (Fig. 4).
271   The CO molecule volume mixing ratio (VMR) near the mesopause at 75–80 km decreased
272   from 10 ppmv of background level to 4 ppmv on 19–21 February (Fig. 3a), when the sharp
273   vertical CO gradient at the lower edge of the CO layer near about 6 ppmv increased in height
274   by about 8 km (between 75 km and 83 km, thick part of the white curve in Fig. 3a). For
275   comparison, the pre- and post-SSW vertical variations of the 6-ppmv contour were observed in
276   a range 2–3 km (white curve in Fig. 3a). Moreover, similar variations in the zonal mean 6-
277   ppmv level are much weaker (yellow curve in Fig. 3e). This indicates that local and regional
278   mesosphere over the MWR site was disturbed by some source acted during the SSW, which is
279   identified below. We take here the 6-ppmv contour as a conditional lower edge of the CO layer
280   since the CO gradients sharply increase from 0.2–0.3 ppmv km^{-1} in a 10-km layer below to

281   0.6–0.8 ppmv km^{-1} in a 10-km layer above (below and above the white curve in Fig. 3a). The

282   similar gradient change is a characteristic of the mesospheric CO profiles in boreal winter from

283   ground-based and satellite observations (Fig. 4 in Koo et al., 2017; Fig. 5 in Ryan et al., 2017).

284   The local mesospheric CO variability from the MWR observations over Kharkiv agrees

285   with regional one from the MLS data averaged over the adjacent area 47.5–52.5°N, 26–46°E

286   (Fig. 3b, the white curve for 6 ppmv). However, the zonal mean CO profiles in the same zone

287   do not show an anomalous decrease of the mesospheric CO during the SSW (yellow curve in

288   Fig. 3a, 3b and 3e).

289   Unlike the mesosphere, the CO descent and an increase in CO abundance is observed in

290   the stratosphere from both regional and zonal mean MLS data shortly after the SSW start

291   (contour 0.1 ppmv in Fig. 3d and 3g, respectively). The CO-rich air of 0.1–0.5 ppmv, which is

292   typical for the lower mesosphere (Fig. 3c) descended down to about 30 km (Fig. 3d and 3g), far

293   exceeding typical stratospheric CO mixing ratios on the order of about 0.01–0.02 ppmv (Engel

294   et al., 2006; Huret et al., 2006; Funke et al. 2009). The CO-rich stratospheric anomaly is close

295   in time to the wave 1 peak on 10–15 February (solid curve in Fig. 2e), that was observed

296   through the stratosphere down to the 30 km altitude (Fig. 2c).

297   Horizontal distributions of the CO VMR in the Northern Hemisphere at the stratospheric

298   and mesospheric altitudes in Fig. 4 suggest causes of the different CO variability in the

299   stratosphere and mesosphere in Fig. 3. The dynamical deformation, elongation, and

300   displacements of the polar vortex relative to the pole lead to temporal shifts between the low

301   and high CO amounts over the MWR site at Kharkiv (white circle in Fig. 4). The tendency of

302   the planetary wave westward tilt with altitude (dashed lines in Fig. 4, see also Supplemental

303   Figs. S1 and S2 for more details) also contributes to relative zonal shift between the

304   stratosphere and the mesosphere of the low/high CO over Kharkiv.

305   The observed decrease of the local CO in the mesosphere during the SSW (white curve in

306   Fig. 3a) is consistent with the regional data from the satellite observations (white curve in Fig.

307   3b). The decrease is due to the displacement of the CO-rich air to the west relative to Kharkiv

308   (white circle and contours outlined the CO-rich area in Fig. 4a–4c and 4e–4g). This is a result

309   of the dominance of easterlies during the SSW that led to placing of the CO-poor air over

310   Kharkiv with the lowest CO levels on 19–23 February (Fig. 4c and 4g) in correspondence with

311   the MWR (Fig. 3a) and MLS (Fig. 3b) measurements. Recovery to the westerly regime in early

312   March reversed the rotation of the vortex (2–6 March in Fig. 4d and 4h) and caused recovery of

313   high CO level over Kharkiv (since about 1st of March in Fig. 3a and 3b).

314   The polar vortex split influenced the local CO change in the middle stratosphere (Fig. 4m–

315   4o). The low CO level at ~30 km before the SSW start (Fig. 3d) is associated with the relatively

316   distant location of the CO-rich vortex from Kharkiv (Fig. 4m). The vortex split and easterly

317   circulation caused displacement of the small vortex fragment with the CO level higher than 0.1

318   ppmv to Kharkiv just at the SSW start (9–13 February in Fig. 4n) and corresponding sharp CO

319   increase over the Kharkiv region around 30-km altitude (contour 0.1 ppmv in a few days after

320   10 February in Fig. 3d). Vertical CO profiles in Fig. 3c and 3d show that downward penetration

321   of the mesospheric CO-rich air into the startosphere took place around 10 February. As seen

322   from Fig. 4f, 4j, and 4n, the mesospheric CO-rich air appears to be contained inside the small

323   sub-vortex over Kharkiv. The large sub-vortex (Fig. 4n and 4o) contributed to the stratospheric

324   CO increase after 10 February in the zonal mean CO profile near 30 km (Fig. 3g). The two sub-

325   vortices in Fig. 4n and 4o provided a longer duration of the mesospheric intrusion in the zonal

326   mean (Fig. 3g) than a short-time influence of the single sub-vortex in regional data (Fig. 3d).

327   It should be noted that the lower edge of the mid-latitude CO-rich air descended in January

328   – mid-February (dashed lines in Fig. 3d and 3g) similarly to the temperature anomaly in the

329   polar region (Fig. 2a). Descent velocity was about –270 and –220 m·day^{-1} in the case of the

330   regional and zonal mean data, respectively. This is a few times lower than in the vortex region,

331   nevertheless, it is in the range of the winter descent velocity noted above (Ryan et al., 2018).

332   Note also that the vortex split in the CO distribution can be identified only in the middle

333   and upper stratosphere (Fig. 4n and 4o and Fig. S1j and S1k), but not at the stratopause level

334   (Fig. 4j and 4k) and in the mesosphere (Fig. S2, second and third columns for 9–13 and 19–23

335   February 2018, respectively).

336

337

338   **4.2 Zonal wind variability**

339

340   The reversal of the local zonal wind estimated from the CO measurements at the Kharkiv

341   MWR site near the mesopause region was observed. The averaged wind velocity in the altitude

342   range 70–85 km changed between 10 m s^{-1} and –10 m s^{-1} around 10 February (Fig. 5a). After

343   the active phase of the SSW, the zonal wind recovers to the westerly wind and enhances to 20

344   m s^{-1} reaching the highest velocity observed in January–March (Fig. 5a). This zonal wind peak

345   in early March is accompanied by the CO peak at 18 ppmv around 85 km that is also the

346   highest CO abundance over January–March (Fig. 3a). This is closely consistent with the MLS

347   measurements at the 86-km altitude: Kharkiv was located on the 16-ppmv contour in early

348   March (2–6 March in Fig. 4d).

349   During the SSW event, local zonal wind over the station became easterly between the lower

350   stratosphere and lower mesosphere (–30 m s^{-1} up to –40 m s^{-1}, white contours in Fig. 5b). Note

that westerly zonal wind at the stratopause level (~50 km) in January 2018 (mid-winter, the pre-SSW conditions) sometimes increased to more than 100 m s^{-1} (black contours in Fig. 5b).

The recovery of the local westerly wind in the upper mesosphere began in late February (Fig. 5a) and later, in early March, in the lower mesosphere–stratosphere (Fig. 5b). The longer persistence of the westerly anomaly in the stratosphere than at the stratopause level is also seen in the polar region (Fig. 2b). This is a manifestation of the downward migration of the circulation anomalies in the SSW recovery phase, while a near-instantaneous vertical coupling is observed at the SSW start on 10 February (Fig. 2a–2d and Fig. 5).

4.3 Temperature changes

The MLS temperature profiles show that high temperature variability over the Kharkiv region concentrated at the stratopause level, particularly before and during the SSW 2018 (Fig. 6). As known, the SSW events are accompanied by polar stratopause descent to 30–40 km, by stratopause breakdown and subsequent reformation at very high altitudes of about 70–80 km (Manney et al., 2009; Chandran et al., 2011; Limpasuvan et al., 2016; Orsolini et al., 2017). The midlatitude stratopause exhibits less sharp, but significant oscillations between 40 and 50 km in January–first half of February 2018 (dotted curve in Fig. 6) and the highest temperature near –5°C after the SSW start on 12–13 February. The short-time stratopause elevation to the lower-mesospheric altitude ~60 km was observed near 20 February, i.e., close in time to the maximum elevation of the 6-ppmv CO level in the mesosphere (Fig. 3a and 3b). Note that the wave 1 and wave 2 (Fig. 2c–2e), and zonal wind (Fig. 5) do not demonstrate strong anomalies this time. The post-SSW stratopause stabilized at the 50-km altitude and warmed from about –20°C to –10°C (Fig. 6b).

Similarly to the CO profile in Fig. 3, the zonal mean temperature variability is much lower above the stratopause than the regional one (Fig. 6b and 6a, respectively). The stratosphere is equally disturbed in both regional and zonal mean characteristics (Fig. 3d and 3g and Fig. 6a and 6b). This difference may be associated with the influence of the splitted (non-splitted) polar vortex in the stratosphere (mesosphere). The vortex fragments introduce higher local/regional and zonal mean variability in the stratosphere; whereas the vortex region is more uniform in the mesosphere (Fig. 4). That results in the weaker zonal mean variability.

During the SSW, the regional stratospheric temperature in Fig. 6a was warmer by 10–15°C in comparison with the pre- and post-SSW temperature. This is about two times lower warming

385   than in the polar region (Fig. 2a) and about three times lower than it is typically observed

386   during the SSWs (see Section 1). It should be noted that this warm stratospheric anomaly in

387   Fig. 6a (contour –50°C) rapidly descended between the upper and lower stratosphere (dashed

388   arrow) in about 10 days. A similar tendency is seen in Fig. 6b from the zonal mean (contour –

389   55°C) but with a descent within a few days (arrow). So, the SSW start in the midlatitude

390   stratosphere is not accompanied by a near-instantaneous vertical coupling as observed in the

391   polar region (Fig. 2a–2d). Midlatitude stratospheric warming in February 2018 occurred with

392   increasing time lag between the upper and lower stratosphere.

393   As is known, upward propagation of the tropospheric planetary waves into the stratosphere

394   is limited in the easterly zonal wind (Charney and Drazin, 1961). In the changed state of a

395   zonal flow, the critical line for planetary waves (zero wind line) in the polar region descents in

396   a few days that looks like downward propagation of an anomaly from above (Matsuno, 1971;

397   Zhou et al., 2002). Possibly, this process may be delayed in the midlatitude, as seen from Fig.

398   6.

399

5 Discussion

401

402   The observations of the major SSW effects in February 2018 in the NH midlatitude mesosphere

403   by microwave radiometer at the Kharkiv site, Northern Ukraine (50.0°N, 36.3°E), have been

404   provided. The CO altitude profiles in the mesosphere have been measured by the MWR with

405   one-day time resolution. Using the CO molecule as a tracer, the wind speed has been retrieved

406   from the Doppler shift of the CO 115.3 GHz emission and the mesospheric winds reverse from

407   westerly to easterly below the winter mesopause region (70–85 km) has been detected. A few

408   ground-based observations in the mesosphere by the same method have been undertaken at

409   midlatitudes (Sect. 1). The zonal wind and CO profile variability during the major SSW were

410   compared with the daily zonal wind, temperature and zonal wave 1/wave 2 datasets from the

411   MLS data, the ERA-Interim, and MERRA-2 reanalyses. The SSW started with the polar vortex

412   split around 10 February (Fig. 1), zonal wind reverse in the mesosphere and stratosphere (Fig.

413   2b and Fig. 5) and enhanced stratosphere warming and mesosphere cooling (Fig. 2a).

414

5.1 Wave patterns and CO level

416

417   As noted in Sect. 1, CO abundance in the extratropical mesosphere increases with latitude

418   toward the winter pole due to meridional transport. CO accumulation results in the formation of

419   the CO layer with the sharp vertical gradient at its lower edge (Solomon et al., 1985; Shepherd

420 et al., 2014). Because of the horizontal CO gradient at the polar vortex edge, its split and
421 displacement during the SSW cause a significant CO variability at the NH midlatitudes
422 (Solomon et al., 1985; Allen et al., 1999; Funke et al., 2009; Shepherd et al., 2014).

423 In Sect. 4a, based on the MWR observations, we have defined the lower CO edge at 6 ppmv
424 and this edge uplifted during the SSW by about 8 km (between 75 km and 83 km, thick part of
425 the white curve in Fig. 3a). This uplifting noticeably stands out against the pre- and post-SSW
426 variations of the 6-ppmv level occurring within 2–3 km (Fig. 4a). The MLS CO measurements
427 show similar variations in the 6-ppmv level over the Kharkiv region (white curve in Fig. 3b)
428 and their absence in the corresponding zonal mean (yellow curve in Fig. 3a, 3b, and 3e).

429 Mesospheric CO profile uplifting is usually associated with the stratopause elevation
430 during the SSW, when air, poor in CO, enters the mesospheric CO layer from below (Kvissel et
431 al., 2012; Shepherd et al., 2014). Similar ascending motions in the stratopause and mesopause
432 regions were observed in the 2013 SSW from nitric oxide (NO) and showed that the NO
433 contours deflected upwards throughout the mesosphere (Orsolini et al., 2017). Our analysis
434 reveals that the local CO profile variations during the SSW 2018 were closely associated with
435 the changes in the planetary wave patterns in the mesosphere.

436 The MLS CO distribution demonstrates how deformation, elongation (wave 2 effect) and
437 rotation of the CO-rich polar area influence the local CO level over Kharkiv (white circle with
438 respect to the CO contours in Fig. 4a–4h and Fig. S1). The highest elevation of the 6-ppmv CO
439 level in Fig. 3a and 3b corresponds to the lowest CO level over Kharkiv on 19–23 February,
440 when the most distant displacement of the CO contours 16 ppmv and 6 ppmv off the Kharkiv
441 location was observed (Fig. 4c and 4g, respectively; see also the third column in Fig. S1). As
442 known, the strong vertical CO gradient in the winter mesosphere is found at the higher altitudes
443 in the tropics than in the extratropics (Solomon et al., 1985; Allen et al., 1999; Garcia et al.,
444 2014). Then, poleward displacement of the low-latitude air masses is accompanied by the CO
445 abundance decrease and vertical CO gradient elevation at the middle latitudes, as it is observed
446 in Fig. 3a and 3b. A similar effect related to the wave 1 influence was observed during the
447 2003–2004 Arctic warming (Funke et al., 2009): the vortex has shifted from the pole toward
448 the western sector and mid-latitude air poor in CO filled the eastern sector (0–90°E) over 50–
449 80°N and even over the pole.

450 The results of Fig. 4 and Fig. S1 show that meridional displacements of the low-latitude,
451 CO-poor mesospheric air to the Kharkiv region occurred under the planetary wave influence
452 and caused the local CO profile variations in the SSW 2018 (Fig. 3a and 3b). These results,
453 thus, confirm that latitudinal displacements due to wave effects may dramatically affect the
454 local densities of the atmospheric species (Solomon et al., 1985). Figure 6a demonstrates that

455   the local stratopause elevation in February 2018 to about 60 km was relatively small in

456   comparison with the elevation that is characteristic for the polar region, up to 70–80 km

457   (Chandran et al., 2011; Tomikawa et al., 2012; Limpasuvan et al., 2016; Orsolini et al., 2010,

458   2017). No significant stratopause elevation was observed in the zonal mean for 47.5–52.5°N

459   (Fig. 6b). Therefore, the meridional (poleward) and zonal displacements of the CO-rich air

460   masses enclosed within the polar vortex (Solomon et al., 1985; Allen et al., 1999; Funke et al.,

461   2009) rather than stratopause elevation (Kvissel et al., 2012; Shepherd et al., 2014) may be

462   dominant cause of the CO profile uplift observed in the NH midlatitudes during the SSW 2018.

463   In March 2018, after the SSW, vertical CO profile has been re-established (Fig. 3a and 3b)

464   according to the recovery phase following the SSW (Shepherd et al., 2014; Limpasuvan et al.,

465   2016). In the MWR data, the SSW recovery phase in the mesosphere in early March started

466   with the short-term but anomalously high peaks in the local CO (Fig. 3a) and westerly wind

467   (Fig. 5a). These peaks reached the highest values in daily variations of CO and zonal wind over

468   the three months of the observations (January–March). By analogy with the low-CO episode in

469   February discussed above, the high-CO peak in early March 2018 caused by change in the

470   vortex shape and the return of the CO-rich vortex edge region to the Kharkiv location (compare

471   2–6 March in Fig. 4d and 4h with 19–23 February in Fig. 4c and 4g; see also the same dates in

472   Fig. S2).

473   Wind measurements using the CO layer provide a further means to evaluate the validity of

474   the modeled winds. Furthermore, by combining the measurements with ray tracing of gravity

475   wave propagation (e.g. Kogure et al., 2018), this type of measurement may provide specific

476   insights into wave-mean flow interactions, particularly where local temperature inversions alter

477   gravity wave filtering (Hocke et al., 2018; Fritts et al., 2018).

478

479

480   **5.2 Descent of the midlatitude stratospheric anomalies**

481

482   Alternating altitudinal sequence of warm and cool anomalies progressively descended through

483   the mesosphere and stratosphere of the polar region was observed in January–March 2018 (Fig.

484   2a) in consistency with many observations (Zhou et al., 2002; Orsolini et al., 2010; Shepherd et

485   al., 2014; de Wit et al., 2014; Zülicke et al., 2018). The warm anomaly sharply intensified in

486   the stratosphere between 20 and 50 km with simultaneous strong cooling in the mesosphere in

487   the active phase of SSW since 10 February (vertical arrow in Fig. 2a). Unlike this, the

488   midlatitude temperature anomalies do not show the similar vertical arrangement and regular

489   descent with respect to the same mean climatology 2005–2017 (Fig. S3).

During the SSW of 2018, the upper (lower) stratosphere over the Kharkiv region was cooler (warmer) up to 20°C (10°C) than climatological mean with stepwise descent relative to the pre-SSW one (Fig. S3a). However, excluding unstable anomalies at different altitudes, the air temperature through the mesosphere and stratosphere was close to the climatology during most of the time in January–March 2018 (light blue in Fig. S3a). The zonal mean temperature anomalies in Fig. S3b show steady warming of the air in the stratosphere and lower mesosphere and distinct tendency for the anomaly to descend between about 40 km and 20 km during the SSW (20 days, ~ -1 km·day^{-1}). It could be concluded that the temperature anomaly profile observed in the NH midlatitudes may vary in time depending on the observing location and individual SSW event and, thus, differ from climatologically warm (cold) stratospheric (mesospheric) anomaly typical for the SSWs in the NH polar region (e.g. Chandran and Collins, 2014; their Fig. 1g).

The CO profiles in Fig. 3 demonstrate opposite tendencies in the vertical shift of the CO-rich air in the NH midlatitudes. The CO descent in the stratosphere occurred during January–February with velocities of about 270 and 220 m·day^{-1} in a case of the regional and zonal mean data, respectively (Fig. 3d and 3g). In general, this is in a range of the winter descent velocities observed in the polar vortex (Funke et al., 2009; Salmi et al., 2011; Ryan et al., 2018), however, a few times lower than in the polar vortex in the winter 2017–2018 (Fig. 2a). The deepest penetration of the mesospheric CO levels (0.1–0.5 ppmv) to ~30 km was observed immediately after the SSW onset (Fig. 3d and 3g). Although this coincides with the peaks in the wave 1 and wave 2 amplitudes (Fig. 2e), the main reason in the CO increase in the stratosphere over Kharkiv is the location of the small sub-vortex of the split polar vortex (9–13 February, Fig. 4n).

The MLS CO maps in Fig. 4 show that the high CO amount is concentrated inside the polar vortex and its fragments after splitting. This is a result of meridional and downward transport of CO that is strongest in the winter polar vortex (Rinsland et al., 1999; Manney et al., 2009; Kvissel et al., 2012; Shepherd et al., 2014). Before (4–8 February), during (19–23 February) and after (2–6 March) the SSW, Kharkiv was outside the stratospheric vortex/sub-vortices edge (Fig. 4m, 4o and 4p, respectively) and the CO amount was at low level typical for the midlatitude stratosphere (of about 0.01–0.02 ppmv; Engel et al., 2006; Huret et al., 2006; Funke et al. 2009). Descent of the 0.1-ppmv contour marked by dashed lines in Fig. 3d and 3g is observed due to the episodic shift of the vortex edge toward the Kharkiv region or to the corresponding zone 47.5–52.5°N, respectively.

Figure 4 demonstrates that the CO amount inside the polar vortex or its fragments is much higher than in the surrounding area not only in the mesosphere but also in the stratosphere. This leads to the possibility of the enhanced CO appearance even in the stratosphere at about 25–30 km (Engel et al., 2006; Huret et al., 2006; Funke et al., 2009). By analogy, the vortex edge shift beyond the Kharkiv region (Fig. 4c and 4g) resulted in lowering of the regional CO mixing ratios in the mesosphere consistent with both ground-based and satellite observations (Fig. 3a and 3b, respectively). Meridional structure of the mesospheric CO (Sect. 1) provided the uplift of the 6-ppmv level during the SSW relative to pre- and post-SSW levels (Fig. 3a and 3b).

6 Conclusions

The impact of a major sudden stratospheric warming in February 2018 on the mid-latitude mesosphere was investigated using microwave radiometer measurements in Kharkiv, Ukraine (50.0°N, 36.3°E). The zonal wind reversal has been revealed below the winter mesopause region at 70–85 km altitudes during the SSW using the CO profiles. The reverse of the mesospheric westerly from about 10 m s^{-1} to easterly wind about –10 m s^{-1} around 10 February has been documented. The data from the ERA-Interim and MERRA-2 reanalyses and the Aura MLS temperature profiles have been used for the analysis of stratosphere–mesosphere behavior under the SSW conditions. Our local microwave observations in the NH midlatitude combined with the reanalysis data show wide ranges of daily variability in CO, zonal wind and temperature in the mesosphere and stratosphere during the SSW 2018.

Among the most striking SSW manifestations over the midlatitude station in February 2018, there were (i) zonal wind reversal throughout the mesosphere–stratosphere, (ii) oscillations in the vertical profiles of CO, zonal wind and temperature, (iii) descent of the stratospheric CO and temperature anomalies on the time scale of days to months, (iv) wave 2 peak at the vortex split date and (v) strong mesospheric CO and westerly peaks at the start of the SSW recovery phase. Generally, the midlatitude SSW effects are known from many event analyses and in most cases they are associated with zonal asymmetry and polar vortex split and displacements relative to the pole (Solomon et al., 1985; Allen et al., 1999; Yuan et al., 2012; Chandran and Collins, 2014). Our results show that the local midlatitude atmosphere variability in the SSW 2018 includes both the large-scale changes in the zonal circulation and temperature typical for the SSWs and local evolution of the altitude-dependent planetary wave patterns in the individual vortex split event.

The observed local CO variability can be explained mainly by horizontal air mass redistribution due to planetary wave activity with the replacement of the CO-rich air by CO-

558 poor air and vice versa, in agreement with other studies. The MLS CO fields show that the CO-
559 rich air masses are enclosed within the polar vortex. Horizontal (meridional and zonal)
560 displacements of the edge of the vortex or vortex fragments relative to the ground-based
561 midlatitude station may be a dominant cause of the observed CO profile variations during the
562 SSW 2018. The small sub-vortex located over the station at the SSW start caused the
563 appearance of the enhanced CO level not only in the mesosphere but also in the stratosphere at
564 about 30 km. This indicates that the polar vortex contains the CO-rich air masses with much
565 higher CO amount than in the surrounding area and this takes place over the stratosphere–
566 mesosphere altitude range.

567 Microwave observations show that sharp altitudinal CO gradient below the mesopause
568 could be used to define the lower edge of the CO layer and to evaluate oscillation and
569 significant elevation of the lower CO edge during the SSW and its trend on a seasonal time
570 scale. The presented results of microwave measurements of CO and zonal wind in the
571 midlatitude mesosphere at 70–85 km altitudes, which is still not adequately covered by ground-
572 based observations (Hagen et al., 2018; Rüfenacht et al., 2018), are suitable for evaluating and
573 potentially improving atmospheric models. Simulations show that planetary wave forcing by
574 westward propagating wave 1 dominates between 40 and 80 km in the winter polar region
575 during the SSW (Limpasuvan et al., 2016). Our spectral analysis reveals that the westward
576 wave 1 during the SSW 2018 is a dominant wave component through the midlatitude upper
577 stratosphere–mesosphere. Instability of the westward polar jet suggested in previous studies
578 (e.g. Limpasuvan et al., 2016) should be analyzed in the context of the westward wave 1
579 generation in the midlatitude upper stratosphere–mesosphere.

580 Our observation of variability of the CO layer during the SSW deserves further study,
581 particularly in relation to the implications for modelling of wave dynamics and vertical
582 coupling (Ern et al., 2016; Martineau et al., 2018) and chemical processes (Garcia et al., 2014)
583 in the mesosphere.

584

585

586 *Conflict of Interest.* The authors declare that the research was conducted in the absence of any
587 commercial or financial relationships that could be construed as a potential conflict of interest.

588

589 *Author contributions.* GM coordinated and led the efforts for this manuscript. VS initiated the
590 microwave measurements during the SSW event in Kharkiv. VS, DS, VM and AA developed
591 equipment and provided microwave measurements with data processing by AP and DS. GM,

592 VS, YW, OE, AK, and AG analyzed the results and provided interpretation. GM, OE, AK, VS,
593 and WH wrote the paper with input from all authors.
594
595

596 *Acknowledgments.* This work was supported in part by the Institute of Radio Astronomy of the
597 National Academy of Sciences of Ukraine; by Taras Shevchenko National University of Kyiv,
598 project 19BF051-08; by the College of Physics, International Center of Future Science, Jilin
599 University, China. The microwave radiometer data have been processed using ARTS and
600 Qpack software packages (http://www.radiativetransfer.org/). Daily datasets from ERA-Interim
601 reanalysis of European Centre for Medium-Range Weather Forecast (ECMWF) were
602 downloaded from https://www.ecmwf.int/en/forecasts/datasets/archive-datasets/reanalysis-
603 datasets/era-interim. The Aura Microwave Limb Sounder (MLS) measurements of air
604 temperature and CO were obtained from https://mls.jpl.nasa.gov/data/readers.php. Zonal waves
605 were analyzed using the National Oceanic and Atmospheric Administration National Centers
606 for Environmental Prediction, Global Data Assimilation System–Climate Prediction Center
607 (NOAA NCEP GDAS–CPC) data at
608 https://www.cpc.ncep.noaa.gov/products/stratosphere/strat-trop/ and the MERRA-2 data from
609 the National Aeronautics and Space Administration Goddard Space Flight Center, Atmospheric
610 Chemistry and Dynamics Laboratory (NASA GFC ACDL) site at https://acd-
611 ext.gsfc.nasa.gov/Data_services/met/ann_data.html. Authors thank the two anonymous
612 reviewers for their valuable comments and useful suggestions.

613
614

615 **References**
616

617 Alexander, S. P. and Shepherd, M. G.: Planetary wave activity in the polar lower stratosphere,
618   Atmos. Chem. Phys., 10, 707–718, https://doi.org/10.5194/acp-10-707-2010, 2010.
619 Allen, D. R., Stanford, J. L., López-Valverde, M. A., Nakamura, N., Lary, D. J., Douglass, A.
620   R., Cerniglia, M. C., Remedios, J. J., and Taylor F. W.: Observations of middle atmosphere
621   CO from the UARS ISAMS during the early northern winter 1991/92, J. Atmos. Sci., 56,
622   563–583, 1999.
623 Baldwin, M. P. and Dunkerton, T. J.: Stratospheric harbingers of anomalous weather regimes,
624   Science, 294, 581–584, doi:10.1126/science.1063315, 2001.

Buehler, S. A., Mendrok, J., Eriksson, P., Perrin, A., Larsson, R., and Lemke, O.: ARTS, the atmospheric radiative transfer simulator – version 2.2, the planetary toolbox edition, Geosci. Model Dev., 11, 1537–1556, doi:10.5194/gmd-11-1537-2018, 2018.

Butler, A. H. and Gerber, E. P. Optimizing the definition of a sudden stratospheric warming, J. Climate, 31, 2337–2344, doi:10.1175/JCLI-D-17-0648.1, 2018.

Butler, A. H., Seidel, D. J., Hardiman, S. C., Butchart, N., Birner, T., and Match, A.: Defining sudden stratospheric warmings, Bull. Amer. Meteor. Soc., 96, 1913–1928, doi:10.1175/bams-d-13-00173.1, 2015.

Butler, A. H., Sjoberg, J. P., Seidel, D. J., and Rosenlof, K. H.: A sudden stratospheric warming compendium, Earth Syst. Sci. Data, 9, 63–76, doi:10.5194/essd-9-63-2017, 2017.

Chandran, A. and Collins, R. L.: Stratospheric sudden warming effects on winds and temperature in the middle atmosphere at middle and low latitudes: a study using WACCM, Ann. Geophys., 32, 859–874, doi:10.5194/angeo-32-859-2014, 2014.

Chandran, A., Collins, R. L., Garcia, R. R., and Marsh, D. R.: A case study of an elevated stratopause generated in the Whole Atmosphere Community Climate Model, Geophys. Res. Lett., 38, L08804, doi:10.1029/2010GL046566, 2011.

Charlton, A. J. and Polvani, L. M.: A new look at stratospheric sudden warmings. Part I: Climatology and modeling benchmarks. J. Climate, 20, 449–469, 2007. doi:10.1175/JCLI-D-11-00348.1

Charney, J. G. and Drazin, P. G.: Propagation of planetary-scale disturbances from the lower into the upper atmosphere, J. Geophys. Res., 66, 83–109, doi:10.1029/JZ066i001p00083, 1961.

Dee, D. P., Uppala, S. M., Simmons, A. J., Berrisford, P., Poli, P., Kobayashi, S., Andrae, U., Balmaseda, M. A., Balsamo, G., Bauer, P., Bechtold, P., Beljaars, A. C. M., van de Berg, L., Bidlot, J., Bormann, N., Delsol, C., Dragani, R., Fuentes, M., Geer, A. J., Haimberger, L., Healy, S. B., Hersbach, H., Hólm, E. V., Isaksen, L., Kållberg, P., Köhler, M., Matricardi, M., McNally, A. P., Monge-Sanz, B. M., Morcrette, J.-J., Park, B. K., Peubey, C., de Rosnay, P., Tavolato, C., Thépaut, J.-N., and Vitart, F.: The ERA-Interim reanalysis: configuration and performance of the data assimilation system, Q. J. Roy. Meteor. Soc., 137, 553–597, doi:10.1002/qj.828, 2011.

de la Torre, L., Garcia, R. R., Barriopedro, D., and Chandran, A.: Climatology and characteristics of stratospheric sudden warmings in the Whole Atmosphere Community Climate Model, J. Geophys. Res., 117, D04110, doi:10.1029/2011JD016840, 2012.

de Wit, R. J., Hibbins, R. E., Espy, P. J., Orsolini, Y. J., Limpasuvan, V., and Kinnison, D. E.: Observations of gravity wave forcing of the mesopause region during the January 2013

660   major Sudden Stratospheric Warming, Geophys. Res. Lett., 41, 4745–4752,

661   doi:10.1002/2014GL060501, 2014.

662   Di Biagio, C., Muscari, G., di Sarra, A., de Zafra, R. L., Eriksen, P., Fiocco, G., Fiorucci, I.,

663   and Fuà, D.: Evolution of temperature, O_3, CO, and N_2O profiles during the exceptional

664   2009 Arctic major stratospheric warming as observed by lidar and millimeter wave

665   spectroscopy at Thule (76.5N, 68.8W), Greenland, J. Geophys. Res., 115, D24315,

666   doi:10.1029/2010JD014070, 2010.

667   Engel, A., Möbius, T., Haase, H.-P., Bönisch, H., Wetter, T., Schmidt, U., Levin, I.,

668   Reddmann, T., Oelhaf, H., Wetzel, G., Grunow, K., Huret, N., and Pirre, M.: Observation

669   of mesospheric air inside the arctic stratospheric polar vortex in early 2003, Atmos. Chem.

670   Phys., 6, 267–282, doi:10.5194/acp-6-267-2006, 2006.

671   Eriksson, P., Buehler, S. A., Davis, C. P., Emde, C., and Lemke, O.: ARTS, the atmospheric

672   radiative transfer simulator, version 2, J. Quant. Spectrosc. Radiat. Transfer, 112, 1551–

673   1558, doi: 10.1016/j.jqsrt.2011.03.001, 2011.

674   Eriksson, P., Jiménez, C., and Buehler, S. A.: Qpack, a tool for instrument simulation and

675   retrieval work, J. Quant. Spectrosc. Radiat. Transfer, 91, 47–64, doi:

676   10.1016/j.jqsrt.2004.05.050, 2005.

677   Ern, M., Trinh, Q. T., Kaufmann, M., Krisch, I., Preusse, P., Ungermann, J., Zhu, Y., Gille, J.

678   C., Mlynczak, M. G., Russell III, J. M., Schwartz, M. J., and Riese, M.: Satellite

679   observations of middle atmosphere gravity wave absolute momentum flux and of its

680   vertical gradient during recent stratospheric warmings, Atmos. Chem. Phys., 16, 9983–

681   10019, https://doi.org/10.5194/acp-16-9983-2016, 2016.

682   Feng, W., Kaifler, B., Marsh, D. R., Höffner, J., Hoppe, U.-P., Williams, B. P., and Plane, J. M.

683   C.: Impacts of a sudden stratospheric warming on the mesospheric metal layers, J. Atmos.

684   Solar-Terr. Phys., 162, 162–171, 2017.

685   Forkman, P., Christensen, O. M., Eriksson, P., Urban, J., and Funke, B.: Six years of

686   mesospheric CO estimated from ground-based frequency-switched microwave radiometry

687   at 57° N compared with satellite instruments, Atmos. Meas. Tech., 5, 2827–2841, doi:

688   10.5194/amt-5-2827-2012, 2012.

689   Forkman, P., Christensen, O. M., Eriksson, P., Billade, B., Vassilev, V., and Shulga, V. M.: A

690   compact receiver system for simultaneous measurements of mesospheric CO and O_3,

691   Geosci. Instrum. Method. Data Syst., 5, 27–44, doi:10.5194/gi-5-27-2016, 2016.

692   Fritts, D. C., Laughman, B., Wang, L., Lund, T. S., and Collins, R. L.: Gravity wave dynamics

693   in a mesospheric inversion layer: 1. Reflection, trapping, and instability dynamics, J.

694   Geophys. Res.-Atmos., 123, 626–648, https://doi.org/10.1002/2017JD027440, 2018.

Funke, B., López-Puertas, M., García-Comas, M., Stiller, G. P., von Clarmann, T., Höpfner, M., Glatthor, N., Grabowski, U., Kellmann, S., and Linden, A.: Carbon monoxide distributions from the upper troposphere to the mesosphere inferred from 4.7μm non-local thermal equilibrium emissions measured by MIPAS on Envisat, Atmos. Chem. Phys., 9, 2387–2411, https://doi.org/10.5194/acp-9-2387-2009, 2009.

Garcia, R. R., López-Puertas, M., Funke, B., Marsh, D. R., Kinnison, D. E., Smith, A. K., and González-Galindo, F.: On the distribution of CO_2 and CO in the mesosphere and lower thermosphere, J. Geophys. Res.-Atmos., 119, 5700–5718, doi:10.1002/2013JD021208, 2014.

Gardner, C. S.: Role of wave induced diffusion and energy flux in the vertical transport of atmospheric constituents in the mesopause region, J. Geophys. Res.-Atmos., 123, 6581–6604, https://doi.org/10.1029/2018JD028359, 2018.

Goldsmith, P. F., Litvak, M. M., Plambeck, R. L., and Williams, D. R.: Carbon monoxide mixing ratios in the mesosphere derived from ground-based microwave measurements, J. Geophys. Res., 84, 416–418, 1979.

Hagen, J., Murk, A., Rüfenacht, R., Khaykin, S., Hauchecorne, A., and Kämpfer, N.: WIRA-C: a compact 142-GHz-radiometer for continuous middle-atmospheric wind measurements, Atmos. Meas. Tech., 11, 5007–5024, doi: 10.5194/amt-11-5007-2018, 2018.

Hocke, K., Lainer, M., Bernet, L., and Kämpfer, N.: Mesospheric inversion layers at mid-latitudes and coincident changes of ozone, water vapour and horizontal wind in the Middle Atmosphere, Atmosphere, 9, 171, https://doi.org/10.3390/atmos9050171, 2018.

Hoffmann, C. G., Raffalski, U., Palm, M., Funke, B., Golchert, S. H. W., Hochschild, G., and Notholt, J.: Observation of strato-mesospheric CO above Kiruna with ground-based microwave radiometry – retrieval and satellite comparison, Atmos. Meas. Tech., 4, 2389–2408, https://doi.org/10.5194/amt-4-2389-2011, 2011.

Hu, J., Ren, R., and Xu, H.: Occurrence of winter stratospheric sudden warming events and the seasonal timing of spring stratospheric final warming, J. Atmos. Sci., 71, 2319–2334, doi:10.1175/JAS-D-13-0349.1, 2014.

Huret, N., Pirre, M., Hauchecorne, A., Robert, C., and Catoire, V.: On the vertical structure of the stratosphere at midlatitudes during the first stage of the polar vortex formation and in the polar region in the presence of a large mesospheric descent, J. Geophys. Res., 111, D06111, doi:10.1029/2005JD006102, 2006.

Karpechko, A. Yu., Charlton-Perez, A., Balmaseda, M., Tyrrell, N., and Vitart, F.: Predicting sudden stratospheric warming 2018 and its climate impacts with a multimodel ensemble, Geophys. Res. Lett., 24, 13538–13546, https://doi.org/10.1029/2018GL081091, 2018.

Keuer, D., Hoffmann, P., Singer, W., and Bremer, J.: Long-term variations of the mesospheric wind field at mid-latitudes, Ann. Geophys., 25, 1779–1790, doi:10.5194/angeo-25-1779-2007, 2007.

Kogure, M., Nakamura, T., Ejiri, M. K., Nishiyama, T., Tomikawa, Y., and Tsutsumi, M.: Effects of horizontal wind structure on a gravity wave event in the middle atmosphere over Syowa (69°S, 40°E), the Antarctic, Geophys. Res. Lett., 45, 5151–5157. https://doi.org/10.1029/2018GL078264, 2018.

Koo, J.-H., Walker, K. A., Jones, A., Sheese, P. E., Boone, C. D., Bernath, P. F., and Manney, G. L.: Global climatology based on the ACE-FTS version 3.5 dataset: Addition of mesospheric levels and carbon-containing species in the UTLS, J. Quant. Spectrosc. Radiat. Transfer, 186, 52–62, doi:10.1016/j.jqsrt.2016.07.003, 2017.

Kuttippurath, J. and Nikulin, G.: A comparative study of the major sudden stratospheric warmings in the Arctic winters 2003/2004–2009/2010, Atmos. Chem. Phys., 12, 8115–8129, https://doi.org/10.5194/acp-12-8115-2012, 2012.

Kvissel, O. K., Orsolini, Y. J., Stordal, F., Limpasuvan, V., Richter, J., and Marsh, D. R.: Mesospheric intrusion and anomalous chemistry during and after a major stratospheric sudden warming, J. Atmos. Solar-Terr. Phys., 78–79, 116–124, doi:10.1016/j.jastp.2011.08.015, 2012.

Limpasuvan, V., Orsolini, Y. J., Chandran, A., Garcia, R. R., and Smith, A. K.: On the composite response of the MLT to major sudden stratospheric warming events with elevated stratopause, J. Geophys. Res.-Atmos., 121, 4518–4537, doi:10.1002/2015JD024401, 2016.

Manney, G. L., Schwartz, M. J., Krüger, K., Santee, M. L., Pawson, S., Lee, J. N., Daffer, W. H., Fuller, R. A., and Livesey, N. J.: Aura Microwave Limb Sounder observations of dynamics and transport during the record-breaking 2009 Arctic stratospheric major warming, Geophys. Res. Lett., 36, L12815, doi:10.1029/2009GL038586, 2009.

Martineau, P., Son, S.-W., Taguchi, M., and Butler, A. H.: A comparison of the momentum budget in reanalysis datasets during sudden stratospheric warming events, Atmos. Chem. Phys., 18, 7169–7187, https://doi.org/10.5194/acp-18-7169-2018, 2018.

Matsuno, T.: A dynamical model of the stratospheric sudden warming, J. Atmos. Sci., 28, 1479–1494, https://doi.org/10.1175/1520-0469(1971)028<1479:ADMOTS>2.0.CO;2, 1971.

Muscari, G., di Sarra, A., de Zafra, R. L., Lucci, F., Baordo, F., Angelini, F., and Fiocco, G.: Middle atmospheric O_3, CO, N_2O, HNO_3, and temperature profiles during the warm Arctic winter 2001–2002, J. Geophys. Res., 112, D14304, doi:10.1029/2006JD007849, 2007.

Newnham, D. A., Ford, G. P., Moffat-Griffin, T., and Pumphrey, H. C.: Simulation study for measurement of horizontal wind profiles in the polar stratosphere and mesosphere using ground-based observations of ozone and carbon monoxide lines in the 230–250 GHz region, Atmos. Meas. Tech., 9, 3309–3323, doi:10.5194/amt-9-3309-2016, 2016.

Orsolini, Y. J., Limpasuvan, V., Pérot, K., Espy, P., Hibbins, R., Lossow, S., Larsson, K. R., and Murtagh, D.: Modelling the descent of nitric oxide during the elevated stratopause event of January 2013, J. Atmos. Solar-Terr. Phys., 155, 50–61, doi:10.1016/j.jastp.2017.01.006, 2017.

Orsolini, Y. J., Urban, J., Murtagh, D. P., Lossow, S., and Limpasuvan, V.: Descent from the polar mesosphere and anomalously high stratopause observed in 8 years of water vapor and temperature satellite observations by the Odin Sub-Millimeter Radiometer, J. Geophys. Res., 115, D12305, doi:10.1029/2009JD013501, 2010.

Pedatella, N. M., Chau, J. L., Schmidt, H., Goncharenko, L. P., Stolle, C., Hocke, K., Harvey, V. L., Funke, B., and Siddiqui, T. A.: How sudden stratospheric warming affects the whole atmosphere, Eos, 99, https://doi.org/10.1029/2018EO092441, 2018.

Piddyachiy, V., Shulga, V., Myshenko, V., Korolev, A., Antyufeyev, O., Shulga, D., and Forkman, P.: Microwave radiometer for spectral observations of mesospheric carbon monoxide at 115 GHz over Kharkiv, Ukraine, J. Infrared Milli. Terahz. Waves, 38, 292–302, doi:10.1007/s10762-016-0334-1, 2017.

Piddyachiy, V. I., Shulga, V. M., Myshenko, V. V., Korolev, A. M., Myshenko, A. V., Antyufeyev, A. V., Poladich, A. V., and Shkodin, V. I.: 3-mm wave spectroradiometer for studies of atmospheric trace gases, Radiophys. Quantum El., 53(5-6), 326–333. https://doi.org/10.1007/s11141-010-9231-y, 2010.

Rao, J., Ren, R.-C., Chen, H., Liu, X., Yu, Y., and Yang, Y.: Sub-seasonal to seasonal hindcasts of stratospheric sudden warming by BCC_CSM1.1(m): A comparison with ECMWF, Adv. Atmos. Sci., 36, 479–494, doi:10.1007/s00376-018-8165-8, 2019.

Rao, J., Ren, R., Chen, H., Yu, Yu., and Zhou, Y.: The stratospheric sudden warming event in February 2018 and its prediction by a climate system model, J. Geophys. Res.-Atmos., 123, 13332–13345, doi:10.1029/2018JD028908, 2018.

Rinsland, C. P., Salawitch, R. J., Gunson, M. R., Solomon, S., Zander, R., Mahieu, E., Goldman, A., Newchurch, M. J., Irion, F. W., and Chang, A. Y.: Polar stratospheric descent of NO_y and CO and Arctic denitrification during winter 1992–1993, J. Geophys. Res., 104, 1847–1861, 1999.

Rüfenacht, R., Baumgarten, G., Hildebrand, J., Schranz, F., Matthias, V., Stober, G., Lübken, F.-J., and Kämpfer, N.: Intercomparison of middle-atmospheric wind in observations and

800 models, Atmos. Meas. Tech., 11, 1971–1987, https://doi.org/10.5194/amt-11-1971-2018,
801 2018.

802 Rüfenacht, R., Hocke, K., and Kämpfer, N.: First continuous ground-based observations of
803 long period oscillations in the vertically resolved wind field of the stratosphere and
804 mesosphere, Atmos. Chem. Phys., 16, 4915-4925, https://doi.org/10.5194/acp-16-4915-
805 2016, 2016.

806 Rüfenacht, R., Kämpfer, N., and Murk, A.: First middle-atmospheric zonal wind profile
807 measurements with a new ground-based microwave Doppler-spectroradiometer, Atmos.
808 Meas. Tech., 5, 2647–2659, doi:10.5194/amt-5-2647-2012, 2012.

809 Ryan, N. J. Kinnison, D. E., Garcia, R. R., Hoffmann, C. G., Palm, M., Raffalski, U., and
810 Notholt, J.: Assessing the ability to derive rates of polar middle-atmospheric descent using
811 trace gas measurements from remote sensors, Atmos. Chem. Phys., 18, 1457–1474,
812 https://doi.org/10.5194/acp-18-1457-2018, 2018.

813 Ryan, N. J., Palm, M., Raffalski, U., Larsson, R., Manney, G., Millán, L., and Notholt, J.:
814 Strato-mesospheric carbon monoxide profiles above Kiruna, Sweden (67.8°N, 20.4°E),
815 since 2008, Earth Syst. Sci. Data, 9, 77–89, doi:10.5194/essd-9-77-2017, 2017.

816 Salmi, S. M., Verronen, P. T., Thölix, L., Kyrölä, E., Backman, L., Karpechko, A. Yu., and
817 Seppälä, A.: Mesosphere-to-stratosphere descent of odd nitrogen in February–March 2009
818 after sudden stratospheric warming, Atmos. Chem. Phys., 11, 4645–4655,
819 https://doi.org/10.5194/acp-11-4645-2011, 2011.

820 Scheiben, D., Straub, C., Hocke, K., Forkman, P., and Kämpfer, N.: Observations of middle
821 atmospheric H_2O and O_3 during the 2010 major sudden stratospheric warming by a network
822 of microwave radiometers, Atmos. Chem. Phys., 12, 7753–7765,
823 https://doi.org/10.5194/acp-12-7753-2012, 2012.

824 Shepherd, M. G., Beagley, S. R., and Fomichev, V. I.: Stratospheric warming influence on the
825 mesosphere/lower thermosphere as seen by the extended CMAM, Ann. Geophys., 32, 589–
826 608, doi:10.5194/angeo-32-589-2014, 2014.

827 Solomon, S., Garcia, R. R., Olivero, J. J., Bevilacqua, R. M., Schwartz, P. R., Clancy, R. T.,
828 and Muhleman, D. O.: Photochemistry and transport of carbon monoxide in the middle
829 atmosphere, J. Atmos. Sci., 42, 1072–1083, 1985.

830 Stray, N. H., Orsolini, Y. J., Espy, P. J., Limpasuvan, V., and Hibbins, R. E.: Observations of
831 planetary waves in the mesosphere-lower thermosphere during stratospheric warming
832 events, Atmos. Chem. Phys., 15, 4997–5005, https://doi.org/10.5194/acp-15-4997-2015,
833 2015.

834 Tao, M., Konopka, P., Ploeger, F., Grooß, J.-U., Müller, R., Volk, C. M., Walker, K. A., and
835   Riese, M.: Impact of the 2009 major sudden stratospheric warming on the composition of
836   the stratosphere, Atmos. Chem. Phys., 15, 8695–8715, https://doi.org/10.5194/acp-15-
837   8695-2015, 2015.

838 Taguchi, M.: Comparison of subseasonal-to-seasonal model forecasts for major stratospheric
839   sudden warmings, J. Geophys. Res.-Atmos., 123, 10,231–10,247,
840   doi:10.1029/2018jd028755, 2018.

841 Tomikawa, Y., Sato, K., Watanabe, S., Kawatani, Y., Miyazaki, K., and Takahashi, M.: Growth
842   of planetary waves and the formation of an elevated stratopause after a major stratospheric
843   sudden warming in a T213L256 GCM, J. Geophys. Res., 117, D16101,
844   doi:10.1029/2011JD017243, 2012.

845 Tripathi, O. P., Baldwin, M., Charlton-Perez, A., Charron, M., Cheung, J. C. H., Eckermann, S.
846   D., Gerber, E., Jackson, D. R., Kuroda, Yu., Lang, A., McLay, J., Mizuta, R., Reynolds, C.,
847   Roff, G., Sigmond, M., Son, S.-W., and Stockdale, T.: Examining the predictability of the
848   stratospheric sudden warming of January 2013 using multiple NWP systems, Mon. Weather
849   Rev., 144, 1935–1960, doi:10.1175/mwr-d-15-0010.1, 2016.

850 Vargin, P. N. and Kiryushov, B. M.: Major sudden stratospheric warming in the Arctic in
851   February 2018 and its impacts on the troposphere, mesosphere, and ozone layer, Russian
852   Meteorology and Hydrology, 44, 112–123, doi:10.3103/S1068373919020043, 2019.

853 Waters, J. W., Wilson, W. J., and Shimabukuro, F. I.: Microwave measurement of mesospheric
854   carbon monoxide, Science, 191, 1174–1175, doi:10.1126/science.191.4232.1174, 1976.

855 WMO Commission for Atmospheric Sciences. Abridged Final Report of the Seventh Session,
856   Manila, 27 February – 10 March, 1978. WMO-No. 509, 113 p., available at:
857   http://library.wmo.int/pmb_ged/wmo_509_en.pdf, 1978.

858 Xu, X., Manson, A. H., Meek, C. E., Chshyolkova, T., Drummond, J. R., Hall, C. M., Riggin,
859   D. M., and Hibbins, R. E.: Vertical and interhemispheric links in the stratosphere-
860   mesosphere as revealed by the day-to-day variability of Aura-MLS temperature data, Ann.
861   Geophys., 27, 3387–3409, doi:10.5194/angeo-27-3387-2009, 2009.

862 Yu, Y., Cai, M., Shi, C., and Ren, R.: On the linkage among strong stratospheric mass
863   circulation, stratospheric sudden warming, and cold weather events, Mon. Weather Rev.,
864   146, 2717–2739, doi:10.1175/MWR-D-18-0110.1, 2018.

865 Yuan, T., Thurairajah, B., She, C. Y., Chandran, A., Collins, R. L., and Krueger, D. A.: Wind
866   and temperature response of midlatitude mesopause region to the 2009 Sudden
867   Stratospheric Warming, J. Geophys. Res., 117, D09114, doi:10.1029/2011JD017142, 2012.

868   Zhou, S., Miller, A. J., Wang, J., and James, K. A.: Downward-propagating temperature

869   anomalies in the preconditioned polar stratosphere, J. Climate, 15, 781–792,

870   doi:10.1175/1520-0442(2002)015<0781:DPTAIT>2.0.CO;2, 2002.

871   Zülicke, C. and Becker, E.: The structure of the mesosphere during sudden stratospheric

872   warmings in a global circulation model, J. Geophys. Res.-Atmos., 118, 2255–2271,

873   doi:10.1002/jgrd.50219, 2013.

874   Zülicke, C., Becker, E., Matthias, V., Peters, D. H. W., Schmidt, H., Liu, H.-L., de la Torre

875   Ramos, L., and Mitchell, D. M.: Coupling of stratospheric warmings with mesospheric

876   coolings in observations and simulations, J. Climate, 31, 1107–1133, doi:10.1175/JCLI-D-

877   17-0047, 1, 2018.

878

879

880

881

882

883

884 **Figure 1.** The polar vortex split at the 10-hPa pressure level during the SSW event in February

885 2018. Geopotential heights are calculated from ERA-Interim reanalysis data.

886

887

888
889
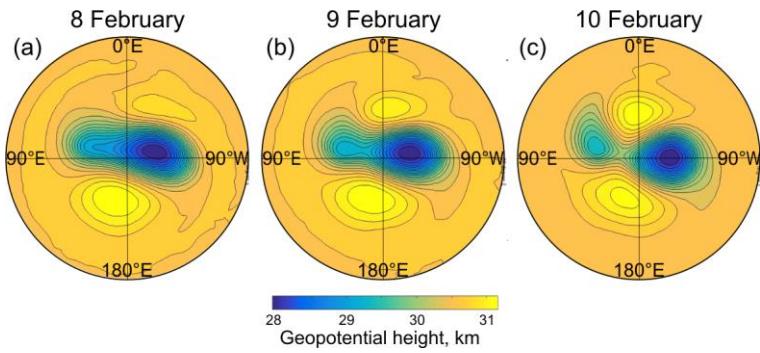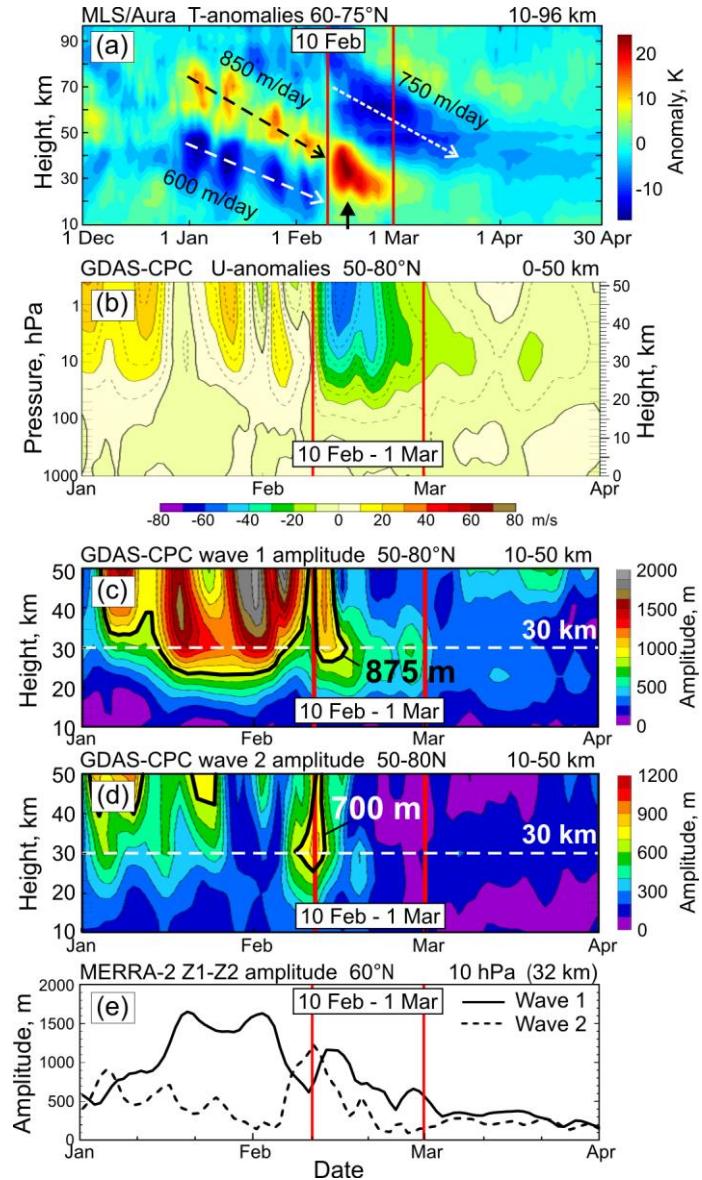
890   **Figure 2.** The development of the SSW in 2018 from the vertical profiles of (a) Aura MLS
891   temperature anomalies in December 2017–April 2018 at polar zone 60–75°N (with respect to
892   the mean climatology 2005–2017), (b) zonal mean zonal wind anomalies, (c) wave 1 and (d)
893   wave 2 amplitudes in geopotential height in January–March by NOAA NCEP GDAS-CPC data
894   (climatology 1981–2010). (e) zonal wave 1 and wave 2 amplitudes in geopotential height at 10
895   hPa, 60°N, by the MERRA-2 time series from the NASA GFC ACDL data. The SSW-related
896   anomalous variability between 10 February and 1 March 2018 is bounded by red vertical lines.

897
898

899
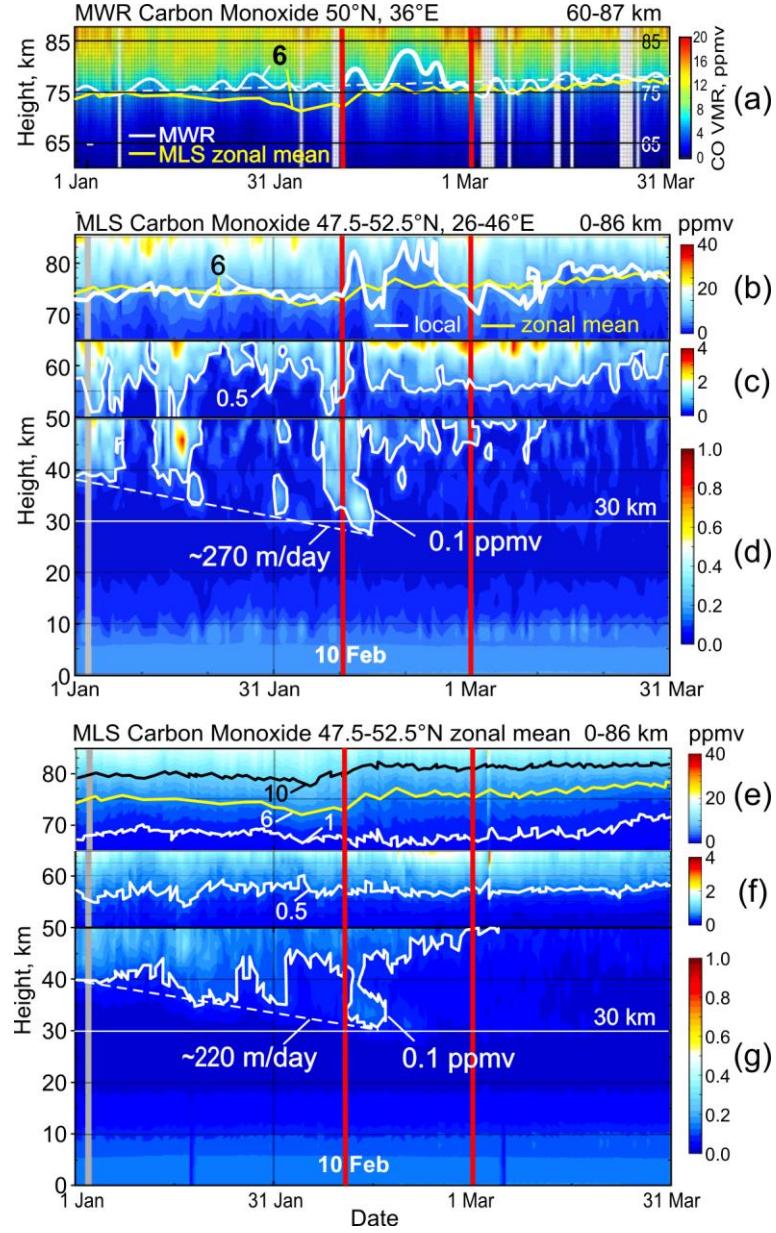
900
901
902 **Figure 3.** (a) Mesospheric CO profile from microwave measurements over Kharkiv averaged
903 in altitude range 70–85 km, and vertical CO profile from the MLS measurements averaged over
904 latitudes 47.5–52.5°N and longitudes (b)–(d) 26–46°E centered at the Kharkiv MWR site
905 (50°N, 36°E) and (e)–(g) 0–360°E for zonal mean. Selected CO levels are highlighted by white,
906 black and yellow contours (see text for details). Data for January–March 2018 are presented
907 and time interval of significant variations in the atmosphere parameters due to the SSW event
908 (from 10 February to 1 March 2018) is bounded by red vertical lines.
909
910

911

912

913

914

915
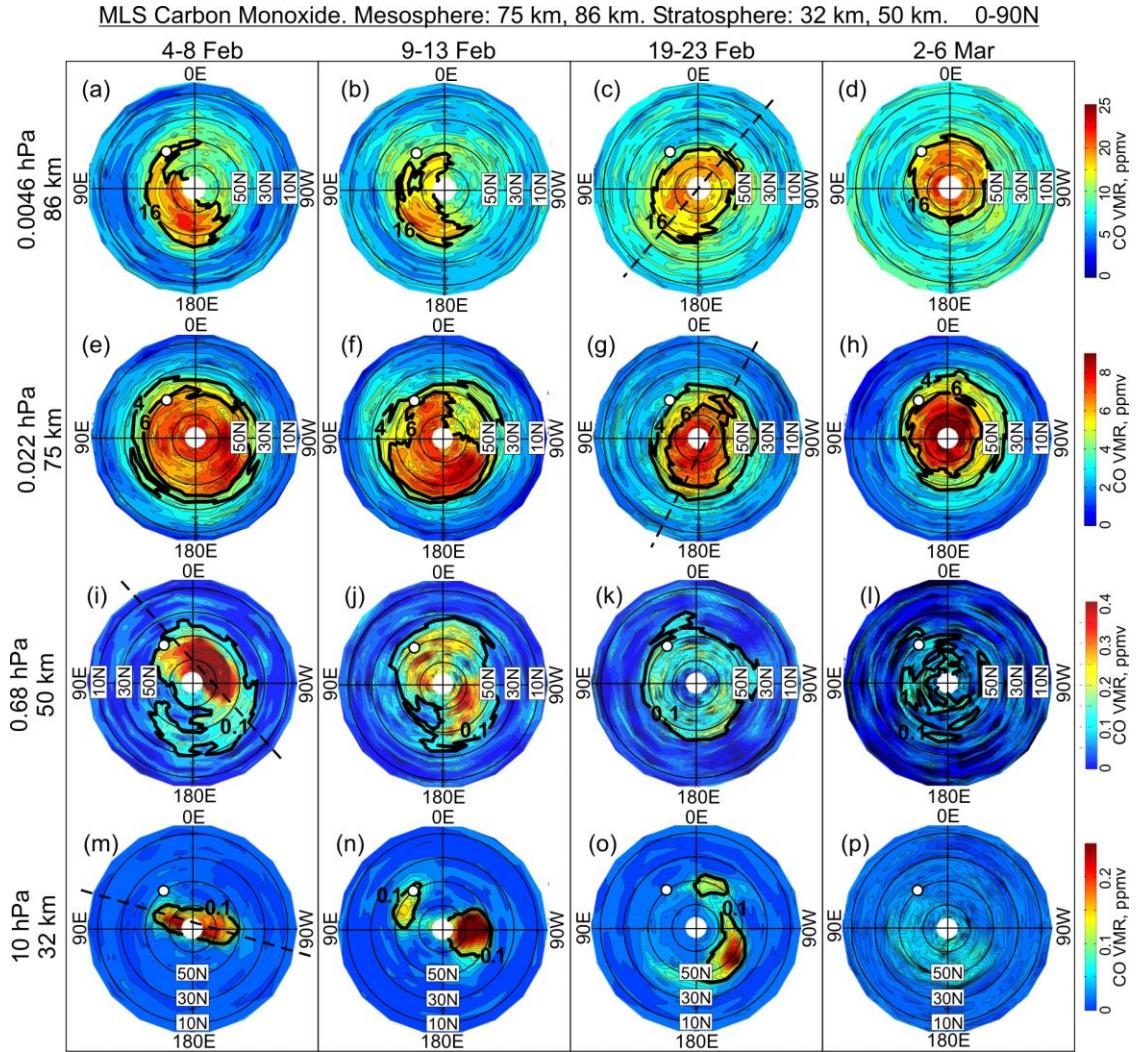
Figure 4. The 5-day mean CO field over the NH (0–90°N) from the MLS measurements at the two mesospheric (75 km and 86 km) and stratospheric (32 km and 50 km) levels before (4–8 February), during (9–13 and 19–23 February) and after (2–6 March) the SSW 2018. White circle shows location of the MWR site Kharkiv relatively the high/low CO amounts marked off by the black contours. Dashed lines indicate clockwise rotation of the elongated polar vortex with altitude as manifestation of upward propagation of planetary waves with their westward tilt with altitude.

923

924

925

926

927

928

929

930

Figure 5. (a) Mesospheric zonal wind microwave measurements over Kharkiv (averaged in altitude range 70–85 km, vertical bars are standard deviations) compared to (b) time-altitude local zonal wind from the ERA-Interim reanalysis data averaged over latitudes 48–52°N and longitudes 34–38°E (centered at the Kharkiv microwave radiometer site, 50°N, 36°E). Time interval of significant variations in the atmosphere parameters due to the SSW event (from 10 February to 1 March, 2018) is bounded by red vertical lines.

937

938

939

940

941

942

943
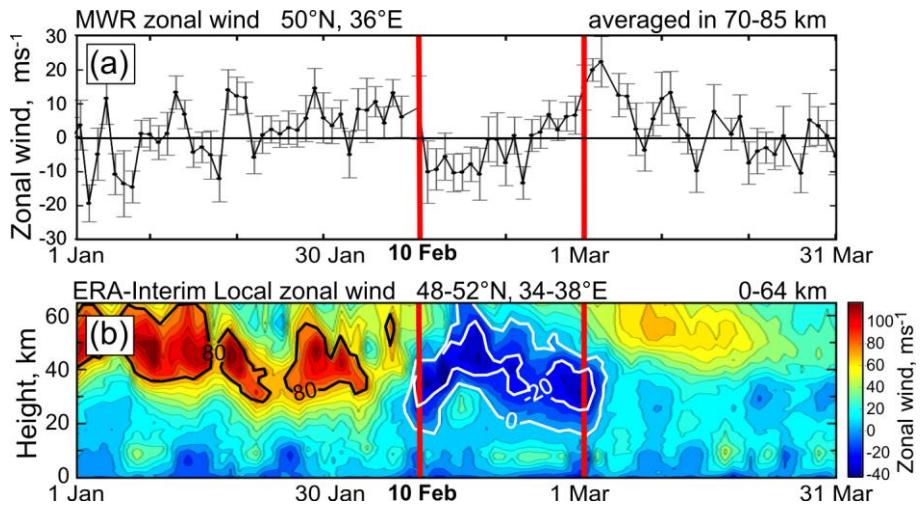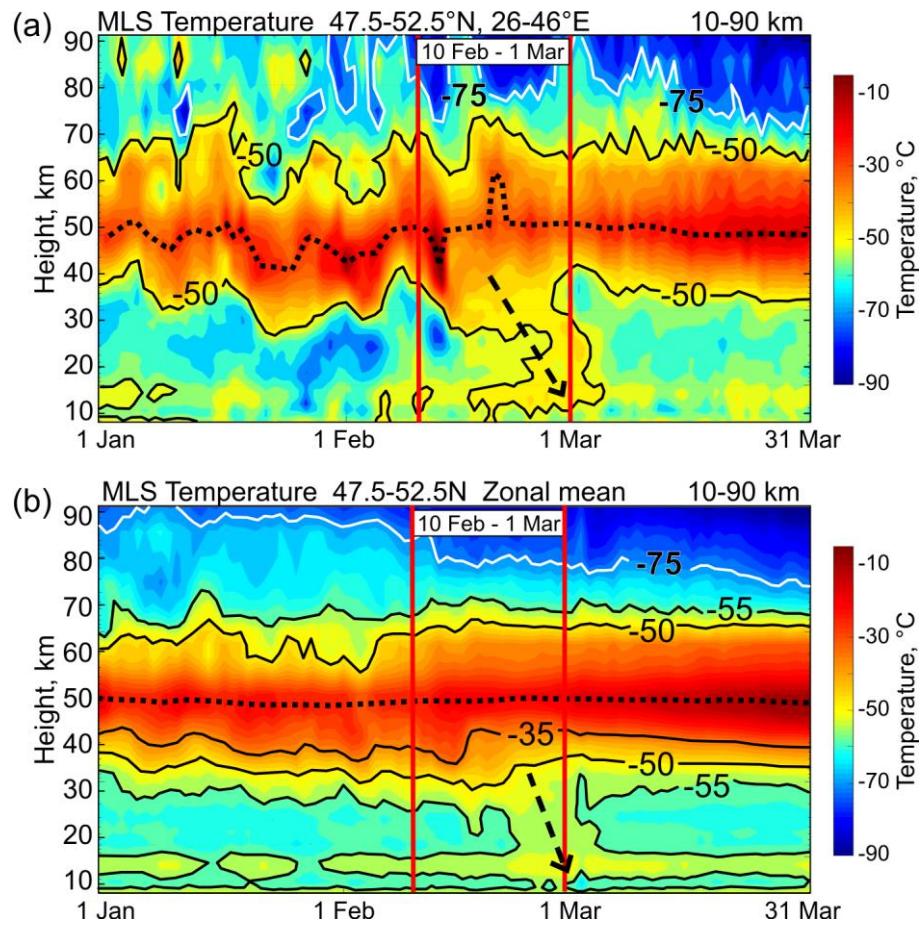
944 **Figure 6.** MLS temperature profiles (a) over the Kharkiv region and (b) zonal average in the

945 zone 47.5–52.5°N. Dashed arrows indicate downward warming.

946

947

948